Electronic Supplementary Material (ESI) for Physical Chemistry Chemical Physics.
This journal is © the Owner Societies 2022

– Supplementary Information for PCCP –

Quantum simulations of thermally activated delayed fluorescence in an all-organic emitter

Tommaso Francese, Arpan Kundu, Francois Gygi and Giulia Galli

Supplementary Sections List:

S1. Molecule: Autocorrelation function of dihedral angle

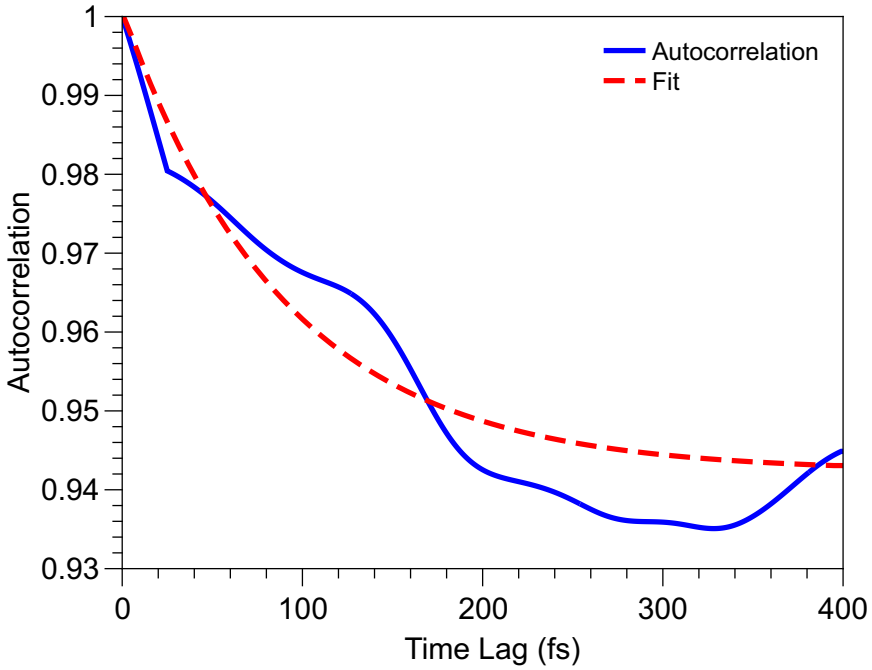

Supplementary Figure 1. Dihedral angle autocorrelation function for a molecular trajectory at T=300 K. The autocorrelation curve was fitted with an exponential decay of the form exp(-x/τ). The resulting τ is 43.6 ± 2.2 fs, which corresponds to ≃ 90 molecular dynamics (MD) steps, where the time-step in our simulations is ≃ 0.4838 fs. Hence by sampling configurations every 90 MD steps or more we obtain a set of statistically non-correlated samples.

S2. Molecule: Pairwise Root-Mean Square Deviation (RMSD)

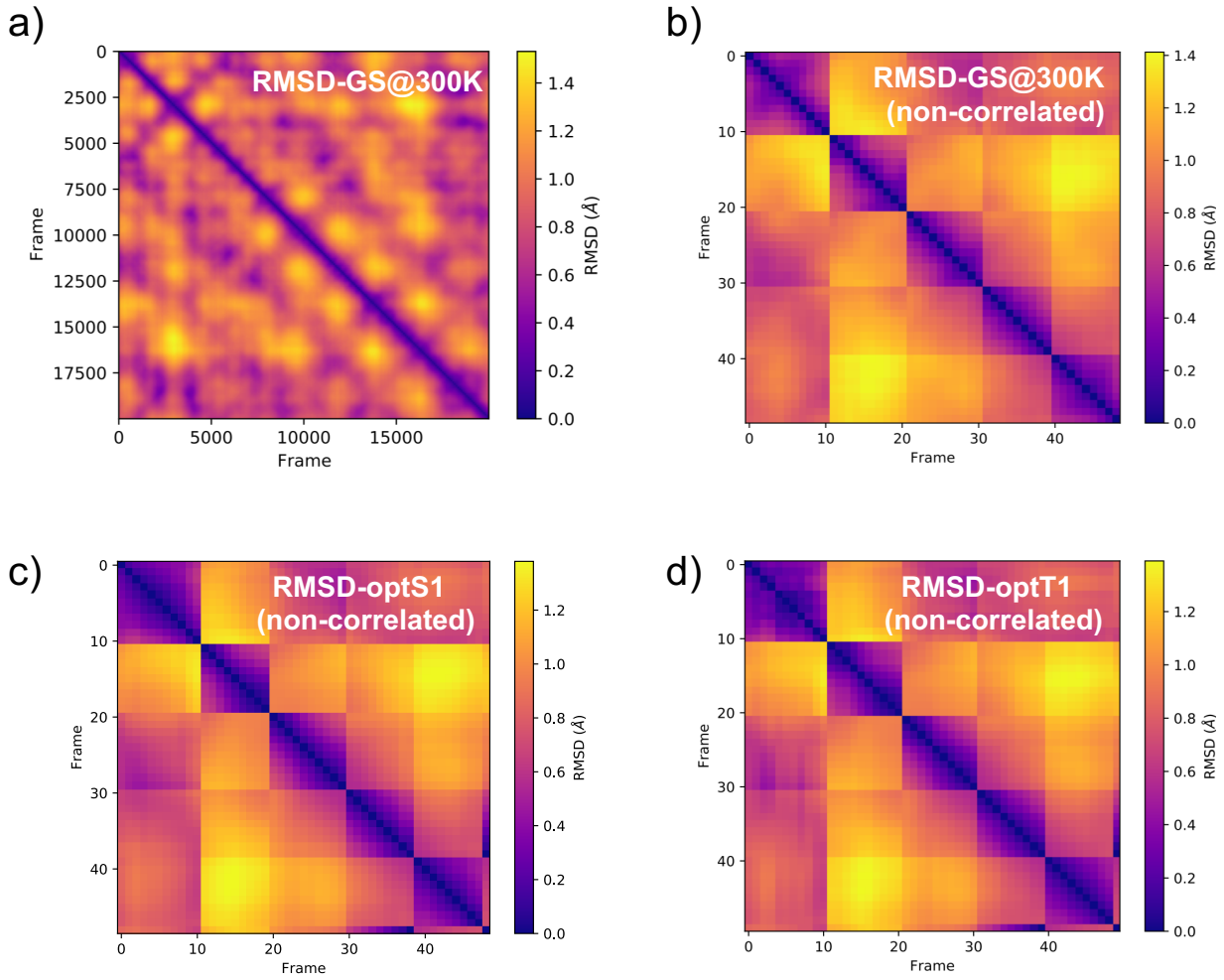

Supplementary Figure 2. The pairwise Root Mean Square Deviation (RMSD)[1,2] computed for a trajectory of 20000 first principles molecular dynamics (FPMD) steps at 300 K. a) Off diagonal regions of low RMSD between two structures suggest that the trajectory is revisiting previously explored states, a necessary condition for obtaining good statistical averages. The same analysis is shown in b) for non-correlated configurations directly extracted from the trajectory at T=300 K (= 50 configurations), showing the occupation of different states as blocks of similar RMSD values along the diagonal. In c) and d) we show the same analysis for the excited state S_1 and T_1 optimized configurations, respectively.

S3. Solid: Distributions of dihedral angles obtained at the PBE and SCAN level of theory

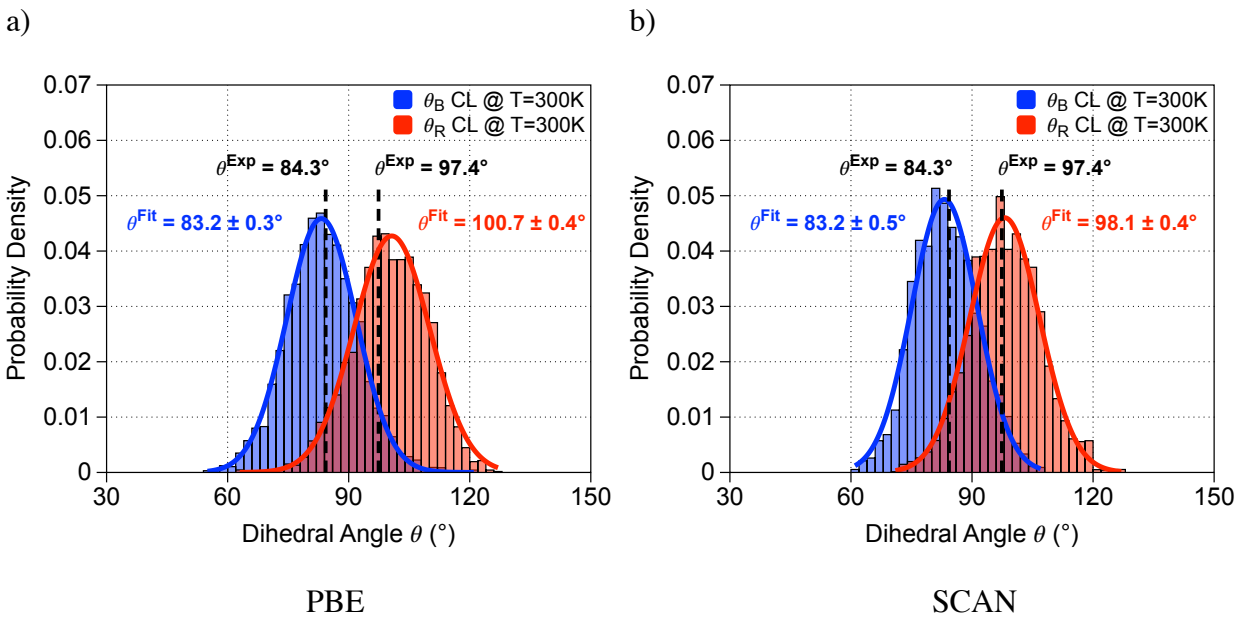

Supplementary Figure 3. Probability distribution of the torsion angles (θ) distributions at finite temperature obtained on classical trajectories at 300 K. Results obtained at the a) PBE and b) SCAN level of theory.

S4. Solid: Autocorrelation function of dihedral angles

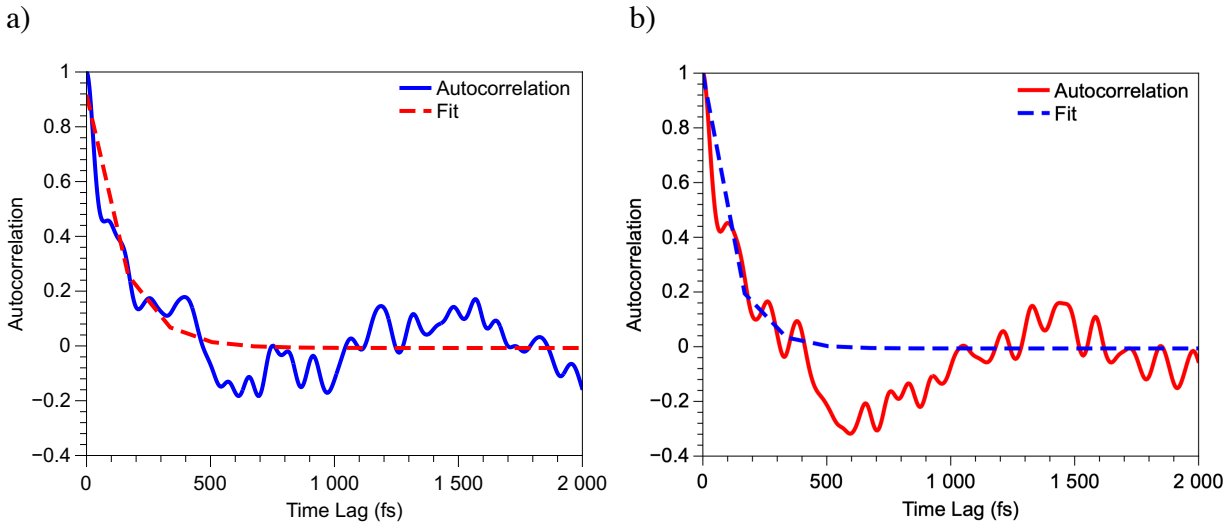

Supplementary Figure 4. Dihedral angle autocorrelation function for a solid trajectory at T=300 K. The autocorrelation curve was fitted with an exponential decay of the form exp(-x/τ). The autocorrelation functions are reported for the pairs of molecules a) #1 (**blue** solid line) and b) #3 (**red** solid line) [see Fig. 2 in the main text]. The resulting τ for molecule #1 is 65 ± 1 fs, which corresponds to ≃134 molecular dynamics (MD) steps and τ for molecule #2 is 51 ± 1 fs, which corresponds to ≃105 MD steps. The time-step in our simulations is ≃ 0.4838 fs. We sampled configurations every 250 steps, generating an ensemble of 84 configurations (see main text)

S5. Solid: Pairwise Root-Mean Square Deviation (RMSD)

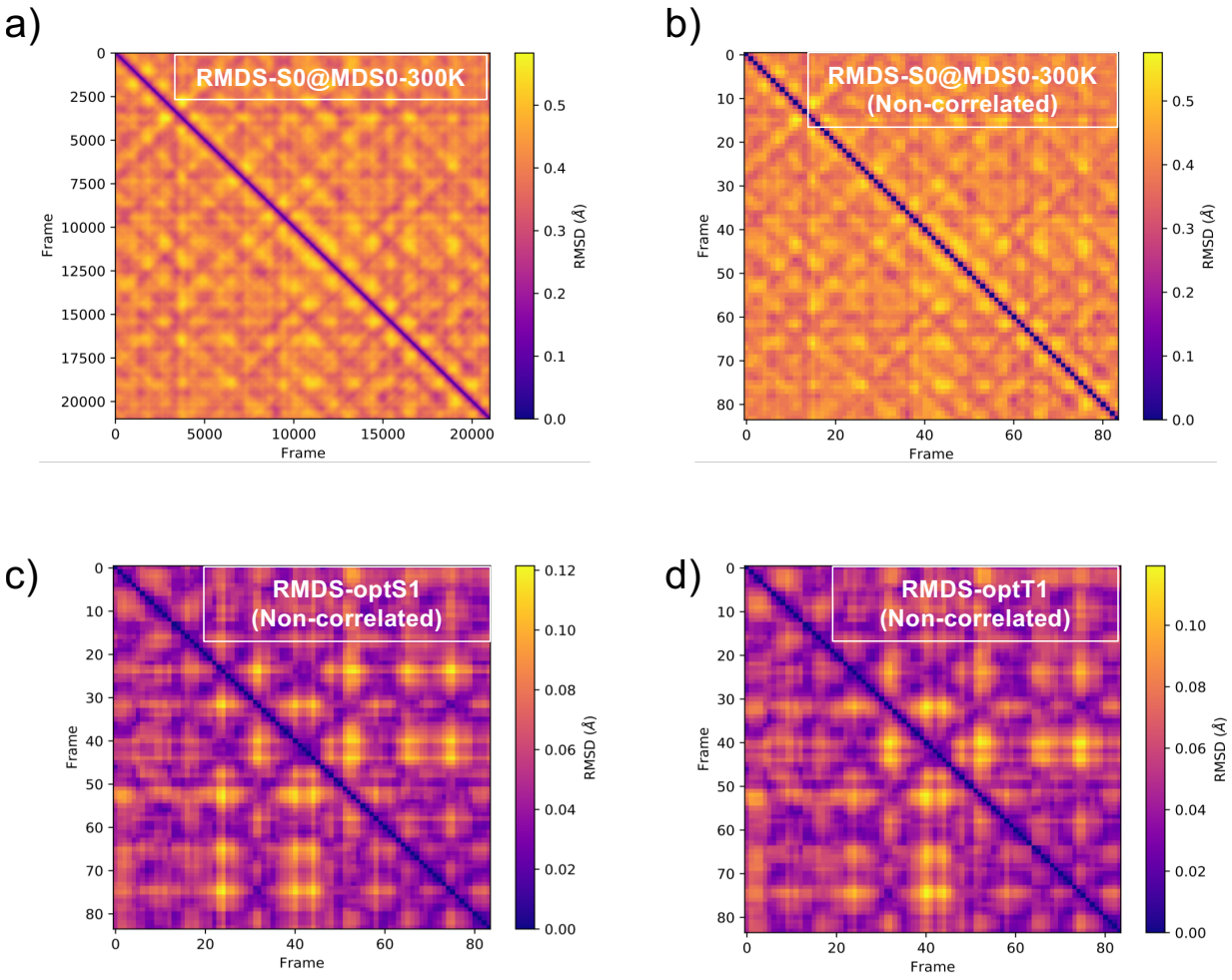

Supplementary Figure 5. The pairwise Root Mean Square Deviation (RMSD)[1,2] computed for a trajectory of 21000 first principles molecular dynamics (FPMD) steps at 300 K a) Off diagonal regions of low RMSD between two structures suggest that the trajectory is revisiting previously explored states, a necessary condition for obtaining good statistical averages. The same analysis is shown in b) for non-correlated configurations directly extracted from the trajectory at T=300 K (84 configurations), showing the occupation of different states as blocks of similar RMSD values along the diagonal. In c) and d) we show the same analysis for the excited state S_1 and T_1 optimized configurations, respectively.

S6. Vibrational Density of States (VDOS)

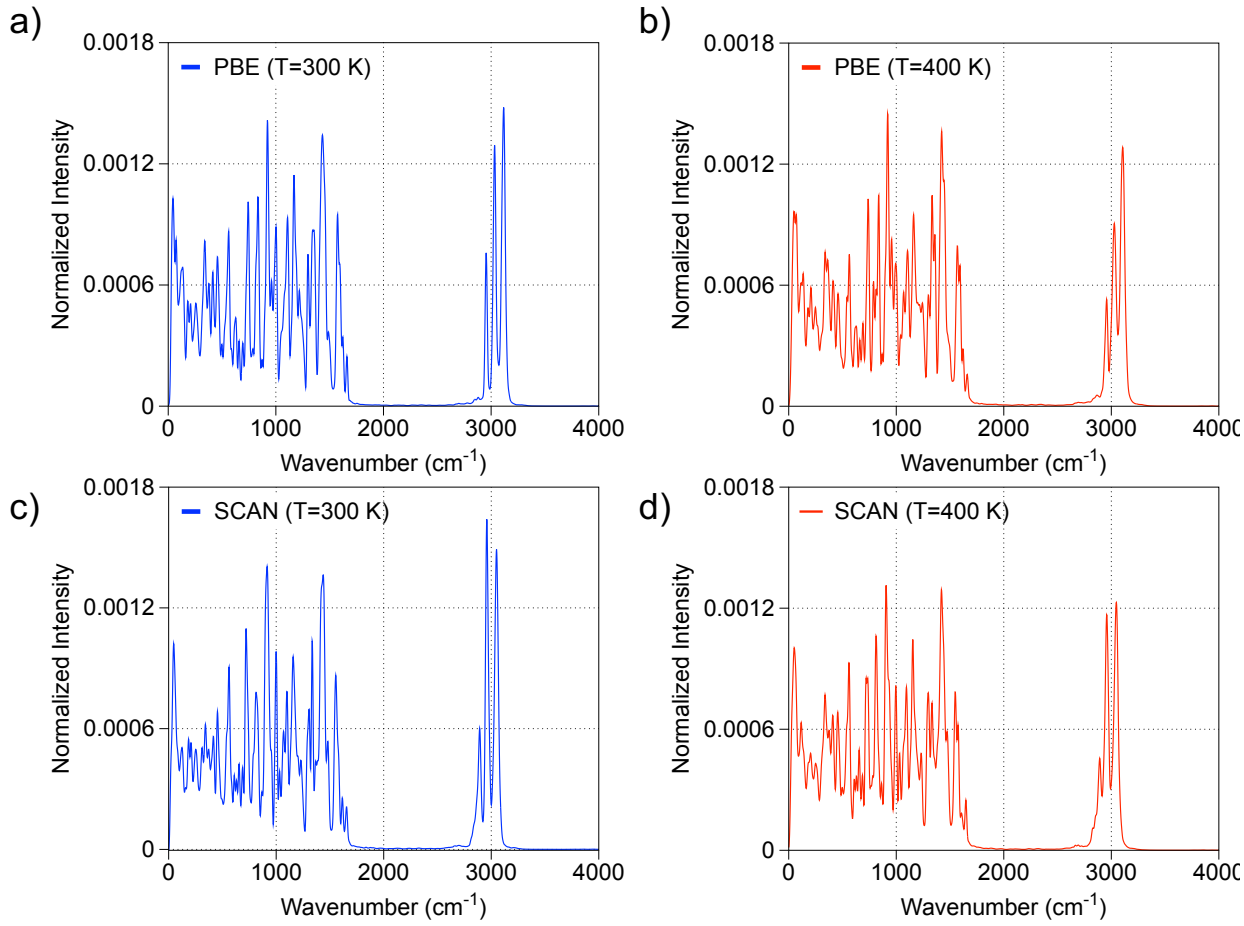

Supplementary Figure 6. The Vibrational Density of States[3-5] (VDOS) calculated for the solid at the PBE and SCAN level of theory at T=300 K are reported in the a) and c) panels, respectively, while the VDOS at T=400 K are reported in b) and d) panels, respectively. The results show that PBE and SCAN yield a similar description of low frequency modes and that temperature has a weak influence on the spectra between 300 and 400 K.

S7. Intersystem Crossing (ISC) and *reverse* Intersystem Crossing (*r*ISC) Data Summary

The direct and reverse intersystem crossing rates between an initial state Ψ_i (*e.g.*, singlet) and a final state Ψ_f (*e.g.*, triplet) were computed with the ORCA code[6]. We report "*verbatim*" the explanation about the rates' calculation given in the Orca manual (newest version v5.0.2, Section 9.39):

"Intersystem crossing (ISC) rate between a given initial state *i* and a final state *f* can be calculated from Fermi's Golden rule:

$$k(\omega)_{if} = \frac{2\pi}{\hbar} \left|\langle \Psi_f | \widehat{H}_{SO} | \Psi_i \rangle\right|^2 \delta(E_i - E_f),$$

which is quite similar to the Equation

$$k(\omega)_{if} = \frac{4\omega^3 n^2}{3\hbar c^3} |\langle \Psi_i | \hat{\mu} | \Psi_f \rangle|^2 \delta\left(E_i - E_f \pm \hbar\omega\right)$$

[…] for Fluorescence, except for the frequency term. The same trick used there can be applied here to switch to the time domain. Then, we are left with a simple time integration, which is not any more difficult to solve than the equations above […]. Orca can use all the infrastructure already presented to compute these ISC rates, including Duschinsky rotation, vibronic coupling effects, use of different coordinate systems and so on. Right now, its use is optimized for CIS/TDDFT […], but it can be applied in general by combining simpler methods to obtain the geometries and Hessians with more advanced methods to compute the SOC matrix elements, when needed."

The Hessian for the initial and final states of every configuration used to estimate the ISC/rISC has been calculated in Orca, starting from the geometries employed obtained from Qbox, after a careful convergence was achieved, both in S_1 and T_1 states. Once Hessians from these geometries in Orca were obtained and employing the total energy differences obtained from Qbox @B3LYP level as input parameter, the non-radiative rates were calculated. In every calculation of the rates the SOC matrix elements and vibrational effects were properly included in order to account for the vibrational effects relevant for light atom elements.

The full set of equations used by Orca for estimating the rates and the methodology therein are reported in the Orca manual (newest version 5.0.2), and in "*de Souza, Neese and Izsak, J. Chem. Phys. 148, 034104 (2018)"* and "*de Souza, Farias, Neese and Izsak, J. Chem. Theory Comput., 15, 3, 1896-1904, (2019)*", respectively.

			I	**II**	**III**	**IV**
	k_{ISC} [s^{-1}]	k_{rISC} [s^{-1}]	k_{rISC} / k_{ISC}	θ@optS$_1$ [°]	θ@optT$_1$ [°]	ΔE_{ST} [eV]
Exp.[7]	2.50 x10^7	4.50 x10^5	0.02	-	-	-
a)	2.93 x10^6	5.63 x10^5	0.20	80.9	75.3	0.28
b)	4.70x10^5	1.43x10^5	0.30	63.0	62.7	0.32
c)	5.80x10^6	8.32x10^4	0.01	73.9	73.9	0.13

Supplementary Table S1. Comparison between experimental and theoretical intersystem crossing (k_{ISC}) and reverse intersystem crossing (k_{rISC}) rates for three configurations: a) equilibrated gas phase molecule at T=0 K, b) a molecule extracted from first principles molecular dynamics trajectories for the molecule at T=300 K, and c) a molecule extracted from first principles molecular dynamics trajectories for the solid at T=300 K which displayed the largest value of the oscillator strength f_{OS}. These rates are all estimated in 'gas phase conditions', *i.e.*, without accounting for any effect from solvent/embedding matrices. In **I**) we show the ratio between *r*ISC and ISC rates; in **II**) the dihedral angle of each optimized model in the singlet excited state (S_1); in **III**) the dihedral angle of each optimized model in the triplet excited state is reported (T_1) and in **IV**) the energy difference between the singlet and triplet state ΔE_{ST}.

$f_{os}\,(Solid)\,/\,f_{os}\,(Gas)$	Absorption	Emission@optS1	Emission@optT1
@PBE	0.3	0.2	0.1
@B3LYP	0.3	0.3	0.2

Supplementary Table S2. Ratio of the oscillator strength (f_{OS}) between high packing (solid)- and gas phase (molecule) limits computed at the PBE and B3LYP level of theory., computed for the singlet (S1) and triplet (T1) states in emission and absorption, at optimized (opt) geometries.

S8. Molecule: HOMO-LUMO Gap Distribution at the PBE Level of theory

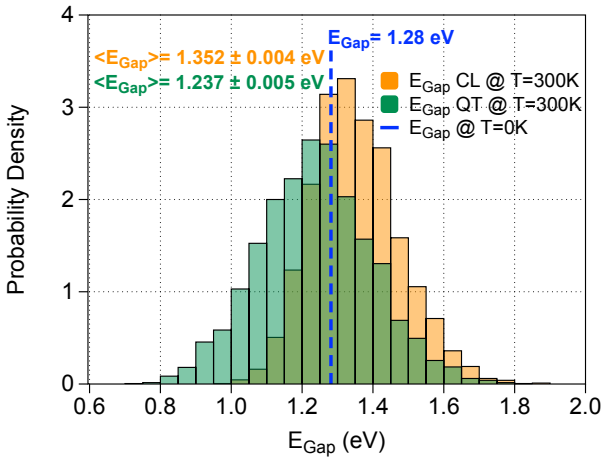

Supplementary Figure 7. Probability distributions of the HOMO-LUMO Gap (E_{Gap}) of the isolated molecule at 300K as obtained on classical (CL) and quantum (QT) trajectories at the PBE level of theory. Averages values are indicated.

S9. Molecule: ΔE_{ST} and f_{OS} distributions for the Classical (CL) and Quantum (QT) sampled configurations at PBE level

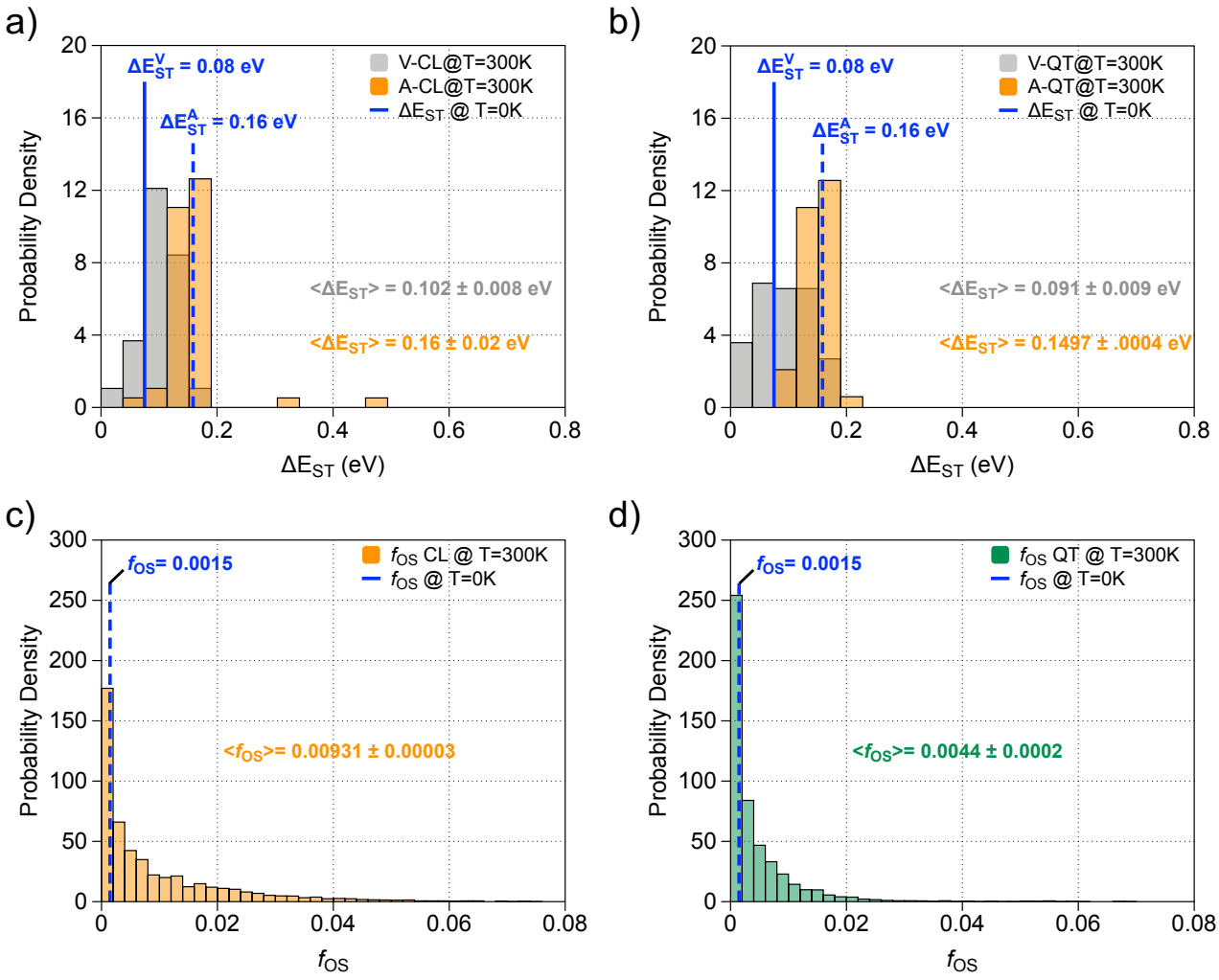

Supplementary Figure 8. Probability distribution of the vertical (V) and adiabatic (A) singlet-triplet energy difference (ΔE_{ST}) at 300 K for classical (a) and quantum mechanical (b) trajectories. Probability distribution of the oscillator strength (f_{OS}) between HOMO and LUMO states of the molecule at 300 K computed on classical (c) and quantum (d) trajectories. The results shown in blue correspond to the values at T=0 K. All data obtained at the PBE level of theory.

S10. Solid: HOMO-LUMO gap as a function of temperature at T=0 K and T=300 K for the high packing fraction system at PBE level.

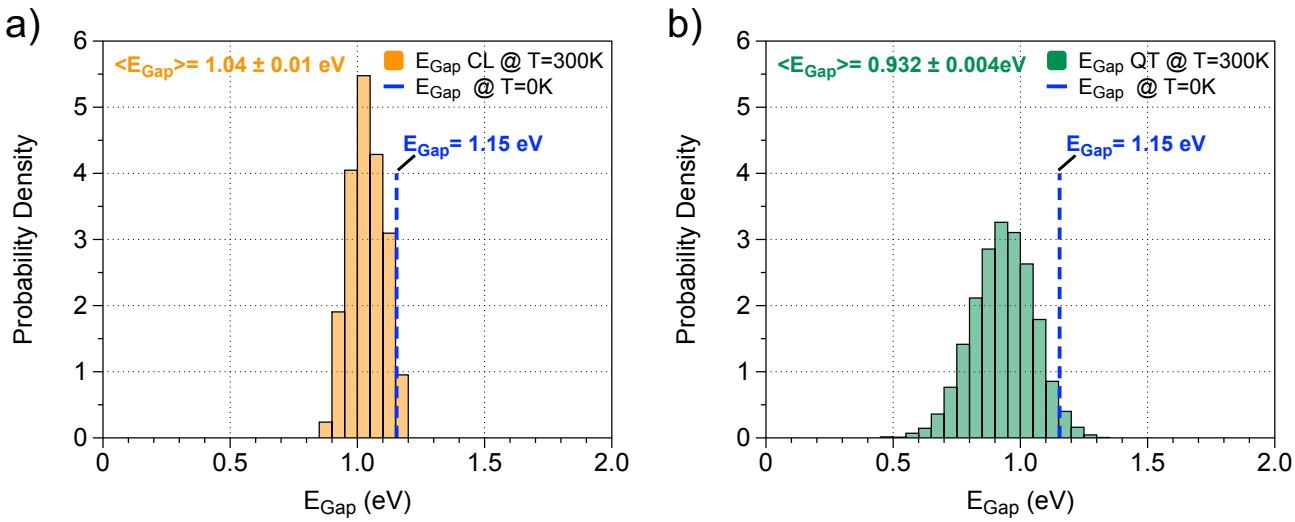

Supplementary Figure 9. Probability distributions of the HOMO-LUMO gap obtained on classical (a) and quantum (b) trajectories at 300 K for the solid. Results obtained at the PBE level of theory.

S11. f_{OS} for the Classical sampled configuration and f_{OS} for the Quantum sampled configurations at PBE level

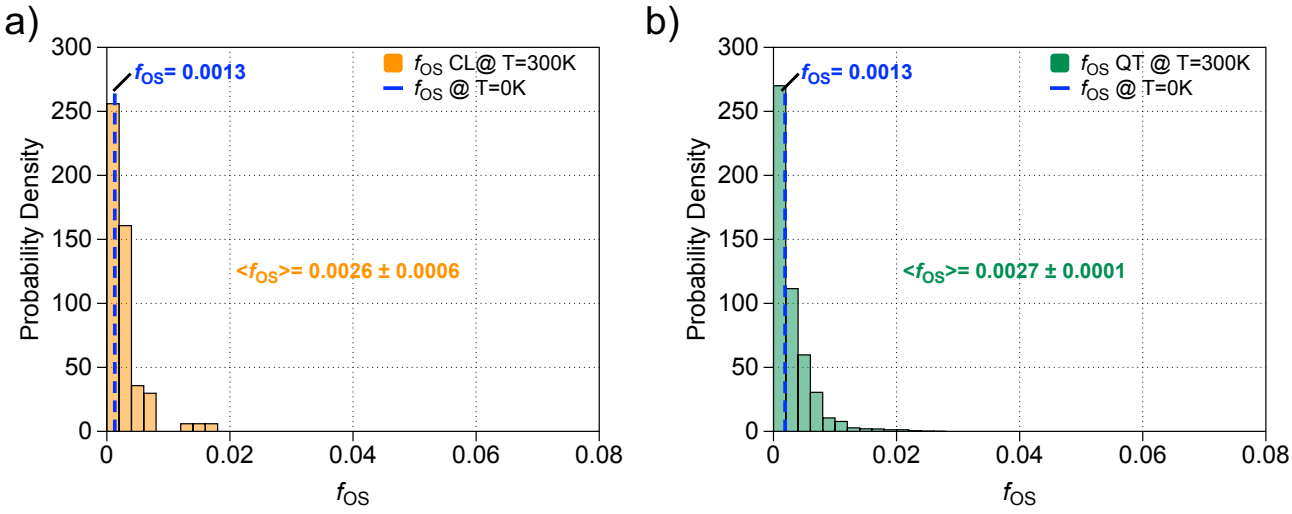

Supplementary Figure 10. *Oscillator strength (f_{OS}) in the solid at finite temperature*. f_{OS} distribution calculated for classical (a) and quantum (b) trajectories at 300 K. Results obtained at the PBE level of theory.

S12. Solid: Polar graph distribution of the ΔE_{ST} for the sampled solid-state configurations from the FPMD and QTMD trajectories calculated at B3LYP level

a) b)

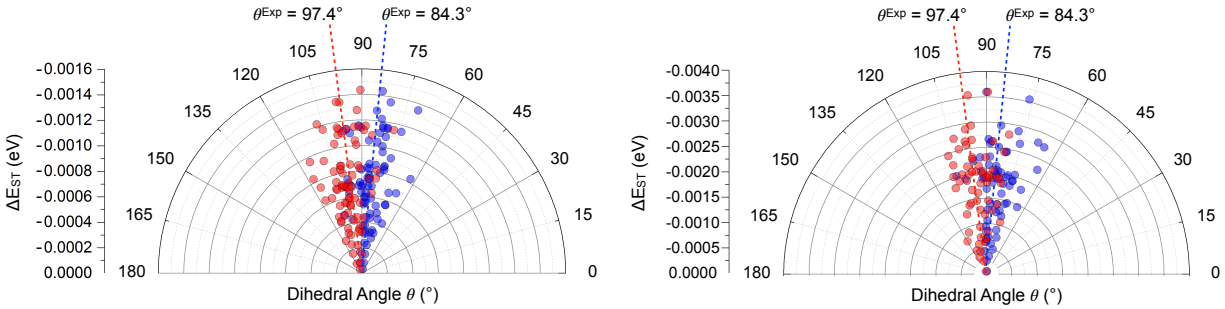

Supplementary Figure 11. Distribution of the energy difference between singlet and triplet (ΔE_{ST}) as a function of the torsion angle θ angle of the 'blue' and 'red' pair of molecules (see Figure 2b of the main text for definition of the two pairs of molecules). a) the ΔE_{ST} vs θ for classical trajectories and b) the ΔE_{ST} vs θ for quantum trajectories.

S13. Solid: Potential transitions at PBE level

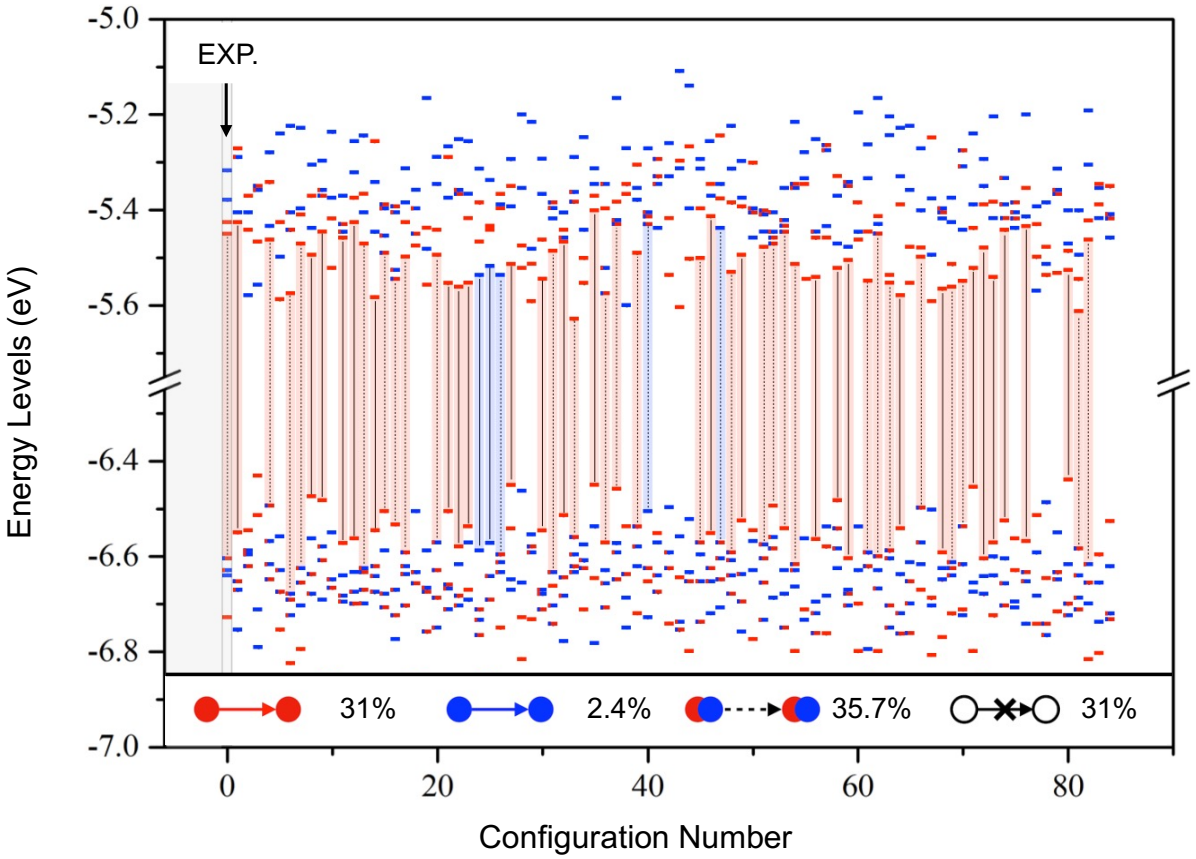

Supplementary Figure 12. The HOMO-LUMO transitions are represented in blue (solid black line with blue contour) when they occur between levels localized on pair 1-2, and in red (solid black line with red contour), when they occur between levels localized on pair 3-4 (see Fig. 2 of the main text for the definition of the pairs of molecules). Mixed transitions are indicated by dashed lines with blue or red contour. The relative percentages of each transition over the whole trajectory are reported at the bottom of the graph. These transitions have been calculated at the PBE level of theory.

S14. Cartesian coordinates of the S_0 optimized structure of the NAI-DMAC in the gas phase limit

73
XYZ file

C	11.766409	10.814050	12.402004
C	12.587904	11.619721	13.215137
C	13.970485	12.100214	12.775286
C	14.307940	11.617499	11.364817
C	13.427602	10.829289	10.596981
C	13.796862	10.443308	9.294465
C	15.023335	10.812462	8.759520
C	15.908913	11.579346	9.512168
C	15.535473	11.969666	10.793941
C	12.107094	11.974958	14.479976
C	10.866809	11.563206	14.956500
C	10.070556	10.757639	14.146701
C	10.515699	10.385258	12.885989
C	15.030373	11.557173	13.764793
C	14.001335	13.648057	12.798305
C	11.330526	9.598583	10.327577
C	10.297626	10.179936	9.536351
C	9.454224	9.311345	8.774654
C	9.669228	7.913207	8.803283
C	10.688687	7.385406	9.576410
C	11.511875	8.227697	10.340013
C	10.069285	11.575535	9.474491
C	9.047604	12.086720	8.700569
C	8.211822	11.230989	7.962209
C	8.408252	9.861320	7.994965
C	8.814872	6.996302	8.010205
C	7.506746	8.982991	7.211465
C	6.906448	6.726898	6.512052
C	5.759986	6.205817	7.095523
C	4.916584	5.380513	6.352876
C	5.196994	5.058985	5.020302
C	6.366423	5.596153	4.460274
C	7.214058	6.420399	5.190168
C	4.285858	4.163088	4.171873
C	3.064199	3.663969	4.955531
C	3.783510	4.960770	2.950426
C	5.082851	2.934974	3.686300
H	13.113323	9.844862	8.696813
H	15.282314	10.497178	7.749374
H	16.875666	11.874255	9.107453
H	16.228907	12.575204	11.377464
H	12.731205	12.598169	15.120333
H	10.531258	11.864148	15.947542
H	9.097082	10.412404	14.493205
H	15.030532	10.460031	13.770773
H	14.827645	11.903942	14.785946
H	16.036285	11.897275	13.487981
H	13.260170	14.062773	12.103601
H	14.989573	14.025572	12.507152
H	13.778975	14.030704	13.802365
H	10.831671	6.305779	9.581225
H	12.307917	7.807848	10.953329
H	10.712501	12.239176	10.049759
H	8.883612	13.162642	8.661570
H	7.397789	11.622473	7.353761
H	5.521380	6.447228	8.130540

H	4.023703	4.988393	6.834797
H	6.626195	5.371253	3.426104
H	8.114771	6.829823	4.734705
H	2.433579	4.493559	5.302512
H	3.355035	3.063247	5.827826
H	2.446809	3.028374	4.306919
H	3.206548	5.840103	3.266080
H	3.134474	4.330308	2.326368
H	4.613418	5.311455	2.324092
H	5.449041	2.343460	4.535946
H	5.950701	3.225175	3.080921
H	4.443817	2.288426	3.068486
H	9.886614	9.751833	12.265159
O	8.984685	5.785598	7.984328
O	6.576929	9.409032	6.541580
N	12.182978	10.434629	11.115363
N	7.773293	7.597341	7.273326

Supplementary Figure 13. Optimized cartesian coordinates of the NAI-DMAC gas phase molecule in the ground state at PBE level of theory.

S15. Cartesian coordinates of the S_0 optimized structure of the NAI-DMAC in the high packing fraction limit

292
XYZ file

C	-0.101602	0.673916	10.442055
C	5.878693	9.339025	10.509105
C	-1.395338	3.810979	6.686170
C	7.168510	6.200158	14.262384
C	-0.120497	2.585933	8.370012
C	5.894039	7.426208	12.580130
C	0.984849	4.284592	6.992564
C	4.788588	5.725380	13.956520
C	-0.261943	2.041839	10.755791
C	6.038618	7.971526	10.194086
C	-0.287664	3.019859	9.715180
C	6.064117	6.993341	11.234644
C	-1.507894	4.846578	5.736297
C	7.281859	5.164161	15.212204
C	0.924470	5.368347	6.095608
C	4.849761	4.641445	14.852893
C	-0.427893	2.453009	12.097097
C	6.203076	7.561418	8.852092
C	7.830980	3.028326	7.001030
C	-2.057655	6.982811	13.947100
C	-0.391062	1.469798	13.189107
C	6.162329	8.543878	7.759870
C	2.211164	3.936923	7.583125
C	3.562220	6.072679	13.366699
C	6.609856	3.246876	6.378189
C	-0.836314	6.764155	14.569783
C	-0.139703	-0.356922	11.502408
C	5.916818	10.370598	9.449533
C	0.033917	1.242353	8.089548
C	5.739943	8.769419	12.861123
C	-3.052667	10.376795	16.081114
C	8.830549	-0.364759	4.868975
C	6.198949	9.297480	0.316464
C	-0.420273	0.711487	20.635212
C	4.311494	-1.804750	18.178244
C	1.464864	11.813241	2.769200
C	-0.514787	4.369790	10.061791
C	6.292139	5.643410	10.887303
C	4.420383	-1.030035	16.929384
C	1.351090	11.034610	4.014883
C	2.175987	9.004744	16.899750
C	3.603482	1.000519	4.052455
C	4.186333	-0.970238	14.509775
C	1.583399	10.971849	6.435340
C	2.098289	6.091301	5.862770
C	3.675889	3.918301	15.085943
C	6.202494	8.705277	1.592839
C	-0.424348	1.303637	19.358837
C	2.277272	8.936533	19.357248
C	3.501880	1.074074	1.594956
C	-0.663059	3.782303	12.400739
C	6.441259	6.232750	8.548345
C	4.373868	0.587660	12.181395
C	1.401892	9.423000	8.768482
C	-1.880380	10.248945	15.329893
C	7.657913	-0.234740	5.619349

C	2.245733	7.513576	19.285280
C	3.533631	2.497032	1.668512
C	2.230545	6.881685	18.052298
C	3.548977	3.126223	2.902553
C	0.027673	0.290363	9.119327
C	5.748410	9.722361	11.831715
C	2.287802	9.677699	18.137497
C	3.490767	0.330580	2.813651
C	1.098887	6.005156	20.845297
C	4.679524	4.005187	0.105851
C	-0.365349	5.803270	5.411382
C	6.139738	4.207232	15.538019
C	7.604201	5.032849	5.122451
C	-1.830109	4.979018	15.826050
C	-0.624853	-0.831594	13.882435
C	6.398184	10.844847	7.067707
C	0.289989	-1.814276	14.238995
C	5.486094	11.829275	6.709983
C	4.883414	8.406504	2.292941
C	0.893780	1.603151	18.657677
C	3.359653	0.807268	13.118144
C	2.415795	9.202386	7.832368
C	2.045439	9.767765	15.645177
C	3.731014	0.231624	5.304488
C	2.292777	9.649282	20.577532
C	3.484417	0.363918	0.373086
C	3.358473	4.673008	7.323828
C	2.415006	5.337038	13.625784
C	2.170537	7.620469	16.863237
C	3.610361	2.384846	4.091085
C	3.806473	8.116065	1.248874
C	1.971144	1.894198	19.702272
C	-3.391869	9.460630	17.258533
C	9.169328	0.550189	3.689969
C	-1.810051	-0.692949	14.605873
C	7.585393	10.705991	6.346967
C	3.258051	0.035728	14.273550
C	2.515280	9.969958	6.674528
C	-0.713913	4.735351	11.375140
C	6.493065	5.279225	9.573361
C	6.492432	4.256017	5.425141
C	-0.718307	5.755278	15.522990
C	3.309575	5.766862	6.462328
C	2.464549	4.243216	14.486385
C	4.267001	-1.864547	20.590233
C	1.510902	11.877853	0.357210
C	-2.065591	-1.521111	15.687882
C	7.842414	11.532936	5.264271
C	4.667248	6.901159	20.559011
C	1.111110	3.107702	0.392136
C	5.189156	-1.222655	13.582180
C	0.583254	11.228341	7.364046
C	4.525737	1.422701	10.914042
C	1.250547	8.588541	10.036391
C	-0.000743	5.901543	19.977446
C	5.779789	4.109435	0.972644
C	4.357924	-1.141162	19.392176
C	1.418825	11.152775	1.554209
C	5.272618	-0.455878	12.430584
C	0.502396	10.465691	8.518711
C	2.702609	7.308731	1.533042
C	3.074373	2.701723	19.416517

C	-1.092436	5.105292	20.303947
C	6.870635	4.906376	0.644554
C	-0.747044	7.216755	5.914630
C	6.522121	2.793270	15.036253
C	7.435477	8.511651	2.219914
C	-1.657225	1.496786	18.731762
C	3.764050	2.750936	11.019639
C	2.012033	7.259989	9.930555
C	5.017613	7.258189	3.301023
C	0.758840	2.751465	17.649065
C	8.619299	9.453058	0.358798
C	-2.840994	0.555380	20.592348
C	-0.135737	5.860482	3.883647
C	5.910604	4.152197	17.065912
C	4.473831	9.676794	3.080356
C	1.303892	0.333126	17.870260
C	-2.213762	8.563251	17.650124
C	7.990935	1.447144	3.298907
C	-3.806533	10.294190	18.485165
C	9.583091	-0.284218	2.463865
C	1.635259	7.159339	0.653021
C	4.142359	2.851480	20.295481
C	5.786405	8.556372	16.844715
C	-0.009211	1.454553	4.103785
C	3.984926	0.612632	9.720472
C	1.792109	9.398505	11.229723
C	8.639726	8.878107	1.625648
C	-2.861579	1.130596	19.324970
C	6.015805	1.716924	10.666450
C	-0.239402	8.295012	10.284236
H	7.920041	2.227680	7.730766
H	-2.146557	7.783403	13.217471
H	2.261489	3.082302	8.251476
H	3.511948	6.929258	12.699988
H	5.756876	2.617684	6.632194
H	0.016720	7.393399	14.315566
H	0.132556	0.922200	7.054477
H	5.639293	9.088566	13.896881
H	-0.551088	5.118576	9.273846
H	6.326379	4.894104	11.674337
H	2.050663	6.960474	5.207649
H	3.723144	3.049392	15.741382
H	-0.826311	4.069117	13.438191
H	6.604669	5.946677	7.510628
H	-1.151174	9.485078	15.585486
H	6.929056	0.528492	5.361639
H	2.249384	5.793803	18.017902
H	3.528339	4.214212	2.940124
H	0.097683	-0.766986	8.883843
H	5.676706	10.779499	12.068415
H	7.497224	5.836140	4.396420
H	-1.723215	4.176425	16.553139
H	-0.681794	10.948306	13.681718
H	6.458617	-0.932619	7.267736
H	2.646415	1.614793	12.972303
H	3.131149	8.396767	7.981067
H	4.979195	11.848167	0.658842
H	0.797470	-1.832797	20.293364
H	4.292801	4.390957	7.803792
H	1.479895	5.620021	13.147355
H	2.139844	7.117486	15.897489
H	3.641054	2.887564	5.056833

H	7.824585	0.076475	14.330542
H	-2.048026	9.937414	6.622669
H	2.466495	0.235228	14.993072
H	3.308159	9.772522	5.955905
H	-0.926274	5.770572	11.626394
H	6.704156	4.243846	9.321472
H	5.540813	4.457633	4.939885
H	0.233153	5.554540	16.008615
H	4.198765	6.363721	6.264416
H	1.575360	3.646304	14.685250
H	6.999987	1.427035	0.683713
H	-1.222084	8.587699	20.263201
H	7.361026	-1.375059	16.241453
H	-1.584996	11.384978	4.710222
H	4.655976	7.337677	19.564157
H	1.121853	2.671131	1.387519
H	4.005988	10.869459	13.769297
H	1.767343	-0.863032	7.177246
H	-0.001272	6.435112	19.031277
H	5.780424	3.577082	1.919342
H	4.444932	-0.056349	19.399584
H	1.330982	10.067803	1.545743
H	6.057080	-0.668607	11.707093
H	-0.280098	10.681066	9.243683
H	2.659217	6.794895	2.489795
H	3.116337	3.215554	18.459236
H	-1.922715	5.022398	19.604376
H	7.701311	4.989986	1.344126
H	7.454686	8.086680	3.221118
H	-1.676275	1.922245	17.730558
H	-3.548453	6.988261	20.719353
H	9.326652	3.020388	0.231266
H	0.796513	6.515119	0.909672
H	4.980036	3.497076	20.038830
H	-0.773768	8.727979	2.155355
H	6.551967	1.281940	18.795792
H	0.042276	7.943998	5.688671
H	5.732959	2.066181	15.262212
H	-0.907755	7.206489	7.000501
H	6.683203	2.802796	13.950487
H	-1.675803	7.559291	5.441545
H	7.450933	2.451422	15.509496
H	3.999848	3.392929	10.161806
H	1.776234	6.617890	10.788018
H	4.027527	3.306043	11.929401
H	1.748503	6.705252	9.020371
H	2.677107	2.600650	11.024984
H	3.098817	7.410248	9.924734
H	5.334956	6.330277	2.809418
H	0.441333	3.679113	18.140671
H	4.064671	7.074459	3.808504
H	1.711359	2.935619	17.141584
H	5.727383	7.512522	4.094260
H	0.048684	2.496402	16.856358
H	0.219447	4.893675	3.504757
H	5.556001	5.119295	17.443745
H	0.606538	6.627622	3.635992
H	5.168322	3.385420	17.315155
H	-1.055660	6.123422	3.348120
H	6.830738	3.889726	17.601439
H	4.353602	10.541046	2.414651
H	1.424015	-0.531021	18.534908

H	5.238746	9.920533	3.828613
H	0.538702	0.089704	17.122005
H	3.516814	9.503964	3.585721
H	2.260645	0.506166	17.364368
H	-1.895727	7.911570	16.828312
H	7.673137	2.099090	4.120719
H	-2.515975	7.911517	18.480932
H	8.292852	2.099090	2.468098
H	-1.346441	9.154501	17.975039
H	7.123709	0.856053	2.973992
H	-1.111643	-1.907411	18.788383
H	6.887726	11.917912	2.161176
H	-4.027623	9.632824	19.334496
H	9.804023	0.376619	1.614006
H	7.548461	-1.990492	18.299423
H	-1.772008	11.999988	2.649606
H	4.907653	9.145611	16.561077
H	0.869435	0.865578	4.387953
H	5.495939	7.901515	17.677641
H	0.281360	2.109674	3.271919
H	6.058719	7.915750	15.998562
H	-0.282160	2.094857	4.950469
H	4.136535	1.144984	8.773245
H	1.640765	8.866576	12.176950
H	2.910789	0.418424	9.830541
H	2.866153	9.592713	11.118595
H	4.487379	-0.358832	9.631041
H	1.289920	10.370445	11.318783
H	6.575301	0.811602	10.406815
H	-0.798742	9.200222	10.543930
H	6.496933	2.175721	11.542096
H	-0.720850	7.836358	9.408787
H	6.106503	2.408130	9.821016
H	-0.330420	7.603642	11.129443
O	4.710301	0.161143	16.907160
O	1.059514	9.843696	4.032875
O	1.765981	9.241604	14.572641
O	4.012536	0.748630	6.380306
O	-0.380849	1.794184	14.372506
O	6.157408	8.219583	6.576630
O	-1.882497	11.339368	11.276290
O	5.773818	11.565216	9.678667
N	2.237107	6.755847	20.491804
N	3.542098	3.253755	0.460929
N	-0.168652	3.548507	7.312716
N	5.940924	6.463159	13.637214
N	-0.386511	0.105579	12.815349
N	6.151270	9.907621	8.133999
N	4.155270	-1.730136	15.732915
N	1.614092	11.731377	5.212411

Supplementary Figure 14. Optimized cartesian coordinates of the NAI-DMAC crystal in the ground state at PBE level of theory.

References

1. N. Michaud-Agrawal, E. J. Denning, T. B. Woolf and O. Beckstein, *Journal of Computational Chemistry*, 2011, **32**, 2319-2327.
2. A. Grossfield, P. N. Patrone, D. R. Roe, A. J. Schultz, D. W. Siderius and D. M. Zuckerman, *Living journal of computational molecular science*, 2018, **1**.
3. M. Brehm and B. Kirchner, *Journal of Chemical Information and Modeling*, 2011, **51**, 2007-2023.
4. M. Brehm, M. Thomas, S. Gehrke and B. Kirchner, *The Journal of Chemical Physics*, 2020, **152**, 164105.
5. M. Thomas, M. Brehm, R. Fligg, P. Vöhringer and B. Kirchner, *Physical Chemistry Chemical Physics*, 2013, **15**, 6608.
6. F. Neese, *Wiley Interdisciplinary Reviews: Computational Molecular Science*, 2012, **2**, 73-78.
7. T. Chen, C.-H. Lu, C.-W. Huang, X. Zeng, J. Gao, Z. Chen, Y. Xiang, W. Zeng, Z. Huang and S. Gong, *Journal of Materials Chemistry C*, 2019, **7**, 9087-9094.